



1 **Reanalysis of the longest mass balance series in Himalaya using nonlinear model: Chhota**
2 **Shigri Glacier (India)**

3 Mohd. Farooq Azam¹, Christian Vincent², Smriti Srivastava^{1,3}, Etienne Berthier⁴, Patrick Wagnon²,
4 Himanshu Kaushik¹, Arif Hussain¹, Manoj Kumar Munda¹, Arindan Mandal⁵, and Alagappan
5 Ramanathan⁶

6 ¹Department of Civil Engineering, Indian Institute of Technology Indore, Simrol, India-453552

7 ²Univ. Grenoble Alpes, IRD, CNRS, INRAE, Grenoble INP, IGE, F-38000 Grenoble, France

8 ³Department of Geography, University of Utah, Salt Lake City, USA

9 ⁴Université de Toulouse, LEGOS (CNES/CNRS/IRD/UT3), Toulouse, 31400, France

10 ⁵Interdisciplinary Centre for Water Research, Indian Institute of Science, Bengaluru 560012, India

11 ⁶School of Environmental Sciences, Jawaharlal Nehru University, New Delhi-110067, India

12

13 Correspondence to: Mohd. Farooq Azam (farooqazam@iiti.ac.in; farooqaman@yahoo.co.in)

14 **Abstract**

15 In-situ glacier-wide mass balances (MB) from traditional glaciological method often carry
16 systematic biases. The glacier-wide MB series on Chhota Shigri Glacier has been reanalysed
17 by combining the traditional MB reanalysis framework and a nonlinear MB model. The
18 nonlinear model is preferred over the traditional glaciological method to compute the glacier-
19 wide MBs as the former can capture the spatiotemporal variability of point MBs from a
20 heterogeneous in-situ point MB network. Further, nonlinear model is also used to detect the
21 erroneous measurements from the point MB observations over 2002–2023. ASTER and
22 Pléiades stereo-imagery show limited areal changes but negative mass balances of -0.38 ± 0.05
23 m w.e. a^{-1} during 2003–2014 and -0.51 ± 0.06 m w.e. a^{-1} during 2014–2020. The nonlinear
24 model outperforms the traditional glaciological method and agrees better with these geodetic
25 estimates. The reanalysed mean glacier-wide MB over 2002–2023 is -0.47 ± 0.19 m w.e. a^{-1} ,
26 equivalent to a cumulative loss of -9.81 m w.e. Our analysis suggests that the nonlinear model
27 can also be used to complete the MB series if for some years the field observations are poor or
28 unavailable. With this analysis, we revisit the glacier-wide MB series of Chhota Shigri Glacier
29 and provide the most accurate and up-to-date version of this series, the longest continuous ever
30 recorded in the Himalaya. We recommend applying the nonlinear model on all traditional
31 glaciological mass balance series worldwide whenever data is sufficient, especially in the
32 Himalaya where in-situ data are often missing due to access issues.

33

34 **1. Introduction**



35 Glaciers are excellent indicators of changing climate; therefore, long-term glacier mass
36 changes are observed to understand the impacts of climate change (Oerlemans, 2001; Zemp et
37 al., 2019). Glacier monitoring is also essential to understand the possible glacial hazards
38 (Harrison et al., 2018; Shukla et al., 2018; Shugar et al., 2021; Gantayat and Ramsankaran,
39 2023), regional hydrology (Azam et al., 2021; Yao et al., 2022; Nepal et al., 2023), and sea
40 level rise (Gardner et al., 2013; Rounce et al., 2023). The glacier mass balance (MB) can be
41 estimated from satellite data, through modelling approaches or measured using field-based
42 traditional glaciological method (Cogley, 2009; Zemp et al., 2015; Kumar et al., 2018; Miles
43 et al., 2021; Berthier et al., 2023).

44 Over the last decade, rapid development has been made through satellite geodetic MB
45 estimates covering almost all glacierized areas in the Himalaya (Brun et al., 2017; Bolch et al.,
46 2019; Shean et al., 2020; Hugonnet et al., 2021; Jackson et al., 2023). These geodetic estimates
47 are primarily available at a multiannual scale and thus cannot be used to understand the inter-
48 annual variability in glacier MB. Conversely, field-based traditional MBs—estimated at
49 annual/seasonal scale—directly respond to local meteorological conditions. Traditional MB
50 observations remain scarce in the Himalaya (Azam et al., 2018). Most observations are
51 available from easily accessible and small glaciers for short periods, generally less than 10-15
52 years.

53 For annual glacier-wide MB estimation, traditional field-based glaciological method
54 has been used in the Himalaya (Azam et al., 2018). This method involves
55 interpolation/extrapolation of point MB measurements from fixed locations to the whole
56 glacier area by applying different approaches, including contouring, profiling, and kriging
57 (Østrem and Brugman, 1991; Zemp et al., 2013) or application of observed MB gradients to
58 the glacier hypsometry (Funk et al., 1997; Wagnon et al., 2021). The selected point
59 measurement sites may not be representative of surrounding areas because (1) ablation stakes
60 are often inserted away from the steep slopes towards the valley walls for safety reasons; thus,
61 the snow avalanche inputs are not included, (2) crevassed areas are not sampled, (3) snow
62 accumulation is site-specific and largely depends on local topography that controls snow
63 blowing/deposition and (4) harsh weather sometimes restricts access to accumulation
64 measurement sites. Almost all the MB series are victims of one or other such issues; therefore,
65 the estimated glacier-wide MBs often carry systematic biases (Thibert et al., 2008). These
66 biases can be corrected by calibrating the MB series using satellite-derived geodetic mass
67 estimates generally over 5-10 years (Zemp et al., 2013; Wagnon et al., 2021).



68 Furthermore, it is practically difficult to keep the position fixed for point measurements
69 due to accessibility, stake displacement due to glacier dynamics, use of different surveying
70 equipment (GPS, dGPS, total station, theodolite, etc.) and different researchers' involvement
71 for decades of monitoring. Hence, the measurement network differs in space and time. In this
72 situation, heterogeneous in-situ measurements do not always allow to catch the large
73 spatiotemporal variability of point MBs; consequently, the point MB-elevation relationship is
74 insufficient to investigate the changes in glacier-wide MBs (Kuhn, 1984; Funk et al., 1997;
75 Huss and Bauder, 2009; Thibert et al., 2013; Vincent and Six, 2013).

76 To include the spatiotemporal variability of point MB measurements, Lliboutry (1974)
77 proposed a linear statistical model and tested it over the small ablation area of Saint Sorlin
78 Glacier (France), assuming similar temporal changes of the MB over the whole area. Vincent
79 et al. (2018) suggested that the linear model of Lliboutry (1974) was valid over a limited
80 elevation range, hence ignoring the decreasing spatiotemporal variability of point MBs with
81 elevation (Oerlemans, 2001). To address this issue, they proposed a nonlinear model that
82 considers the decreasing spatiotemporal changes in point MBs over the large elevation range
83 and successfully tested their model on four different glaciers from different climate regimes,
84 including Chhota Shigri Glacier (India).

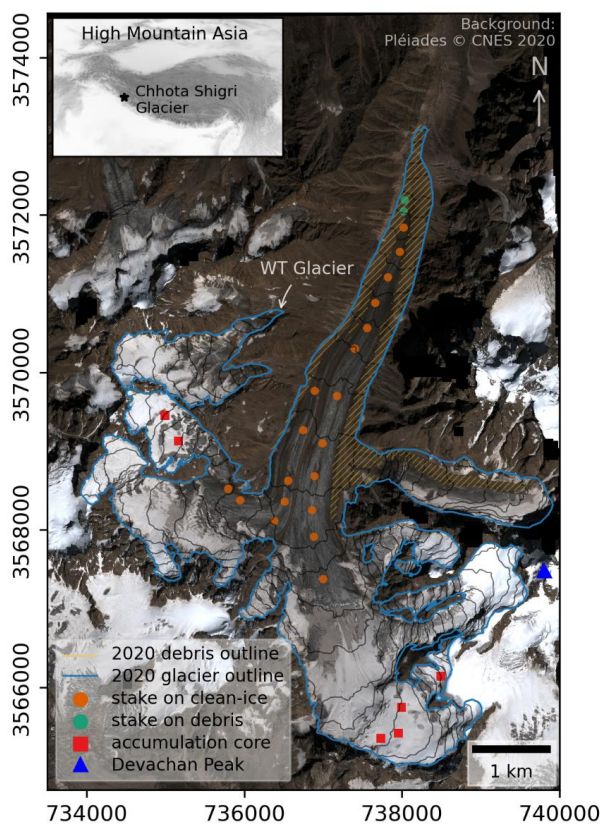
85 In the present study, we apply the nonlinear model to reanalyse the annual MB series
86 of Chhota Shigri Glacier since 2002, the longest series in the Himalaya. Azam (2021)
87 highlighted the importance of Chhota Shigri as a reference glacier for large-scale MB and
88 hydrological studies; therefore, the main aim of the present study is to produce the most
89 accurate glacier-wide MB series in this region. First, the nonlinear model of Vincent et al.
90 (2018) was used to detect the erroneous point MB measurements in the series. Second, the
91 nonlinear model was applied using the observed point MBs to estimate the glacier-wide MB
92 at annual scale. Third, homogenization of the glacier-wide MB series accounting for glacier
93 areal changes was performed; and fourth, the glacier-wide MB series was calibrated using
94 geodetic MBs as recommended by Zemp et al. (2013). Further, we also tested the performance
95 of the nonlinear model to estimate the glacier-wide MB from the snowline at the end of ablation
96 season if no field measurements were conducted in a particular year.

97 **2. Study area**

98 Chhota Shigri Glacier (32.28° N, 77.58° E) is in the Chandra River Basin, a tributary of Upper
99 Indus Basin, Lahaul-Spiti valley of the western Himalaya (Fig. 1). Chhota Shigri flows from
100 5830 to 4100 m a.s.l., with a length of ~9 km and an area of 15.47 km² (in 2020). Based on the



101 most updated map obtained in September 2020, 12% of its total surface area is covered with
102 debris between the snout and 4500 m a.s.l., over medial and lateral moraines from 4100 to
103 ~4900 m a.s.l. and over an eastern tributary glacier (Fig. 1). Debris thickness ranges from less
104 than a few centimetres of thin debris to a few meters of boulders. Valley walls bound its
105 accumulation area, with the highest Devachan peak (6250 m a.s.l.). The accumulation area has
106 two east- and west-oriented tributaries that feed to the main ablation area (<5070 m a.s.l.),
107 having a north aspect and divided into two parallel flows by a medial moraine.



108

109 **Figure 1:** Chhota Shigri Glacier showing the location of ablation and accumulation point
110 measurement sites. Orange strips show the debris-covered glacier area. The background image
111 is a Pléiades satellite image taken on 12 September 2020 (Copyright CNES 2020, Distribution
112 Airbus Defence and Space). The glacier extent corresponds to 12 September 2020. Coordinates
113 are in UTM North, Zone 43.

114

115 Chhota Shigri is a well-studied glacier for various aspects, including traditional MBs,
116 energy balance, dynamics, ice thickness, hydrology, etc. (Wagnon et al., 2007; Azam et al.,
117 2012; Ramsankaran et al., 2018; Haq et al., 2021; Srivastava and Azam, 2022a; Mandal et al.,



118 2020, 2022). Several studies have also observed its geodetic MBs (Berthier et al., 2007;
119 Vincent et al., 2013; Brun et al., 2017; Mukherjee et al, 2018). Long-term annual MBs have
120 been reconstructed over 1950–2020 applying a temperature index model (Srivastava et al.,
121 2022) and over 1979–2020 using an energy balance model (Srivastava and Azam, 2022b). Due
122 to recent glacier wastage on Chhota Shigri Glacier, the western tributary (WT) glacier got
123 disconnected in the summer of 2012 (Srivastava et al., 2022). The fragmented tributary is now
124 clearly visible in the high-resolution Pléiades image from 12 September 2020 (Fig. 1).

125 In this study, we focus on Chhota Shigri Glacier, but the available satellite stereo-
126 images also cover neighbouring Hamtah and Sichum glaciers; therefore, we also estimated the
127 areal changes and geodetic MBs for these two glaciers (sections 3.4 and 3.5). Hamtah Glacier
128 has been studied for its MBs and avalanche contribution (Vincent et al., 2013; Laha et al.,
129 2017). Further, for all three glaciers, we also delineated the debris cover corresponding to 2020
130 (Table 1).

131 3. Methods

132 3.1 Traditional mass balance method

133 Glacier-wide annual MBs (B_a) have been estimated using a network of 22-25 ablation bamboo
134 stakes (inserted up to 10 m inside the glacier) distributed over 4300-4900 m a.s.l. along the
135 main axis of the glacier (Fig. 1), and 4-6 accumulation pits/cores over 5160-5550 m a.s.l
136 distributed over the eastern and western tributaries of the glacier (Wagnon et al., 2007). The
137 traditional glaciological profile method was used to estimate the glacier-wide MB from the
138 observed point MBs (Østrem and Stanley, 1969). First, using the observed point MBs, the mean
139 altitudinal MBs were estimated for each 50-m elevation band from available point MBs within
140 each elevation band (Fig. 1). In case no measurements were available (due to loss of stakes or
141 missing accumulation measurements) the MBs were estimated using linear
142 interpolation/extrapolation of neighbouring bands. Second, the B_a (in m w.e. a⁻¹) was estimated
143 as follows:

$$148 \quad B_a = \frac{1}{S} \sum_{z=mn}^{z=max} b_z s_z, \quad (1)$$

144 where b_z is the mean altitudinal MB (in m w.e. a⁻¹) of a given elevation band, z , of area s_z (m²)
145 and S is the total glacier area (m²). In the ablation area, emergence changes at each ablation
146 stake were converted to the point MB using a fixed density of 900 kg m⁻³ for ice and 350 kg
147 m⁻³ for snow, while in the accumulation area, the varying snow/firn/ice densities (350-900 kg



149 m^{-3}) were measured in the field (Wagnon et al., 2007). The hydrological year for MB
150 calculations is defined from 1 October to 30 September of the following year; however, the
151 exact measurement dates on site varied from a couple of days to a week. Following Thibert et
152 al. (2008), an overall uncertainty of $\pm 0.40 \text{ m w.e. a}^{-1}$ for glacier-wide MB was estimated by
153 incorporating the errors in point measurements and their distribution over the glacier (Azam et
154 al., 2012).

155 Due to access difficulties, snowstorms like on 22-24 September 2018, or logistical or
156 budget issues, some years were under-sampled. This was the case for October 2015, where
157 only two accumulation measurements could be performed, or 2018, where measurements were
158 done early in the season, before the storm. For those two years, point MB data in the
159 accumulation zone, where no measurements had been taken, was estimated using previous
160 years with a similar ablation pattern (Mandal et al., 2020). In 2020, only two in-situ point MB
161 data are available, preventing the traditional method from being applied. Further, no
162 measurements could be performed in 2021; hence, no MB could be estimated. Supplementary
163 Table S1 provides all information about the point MBs and field expeditions since 2002.

164 3.2 Nonlinear mass balance model

165 The nonlinear MB model suggests that the observed point MB, $b_{i,t}$, at any site i for year t , can
166 be decomposed into (1) spatial effect term, α_i , and (2) temporal term, β_t , combined with a
167 spatial effect, γ_i , and can be written as (Vincent et al., 2018):

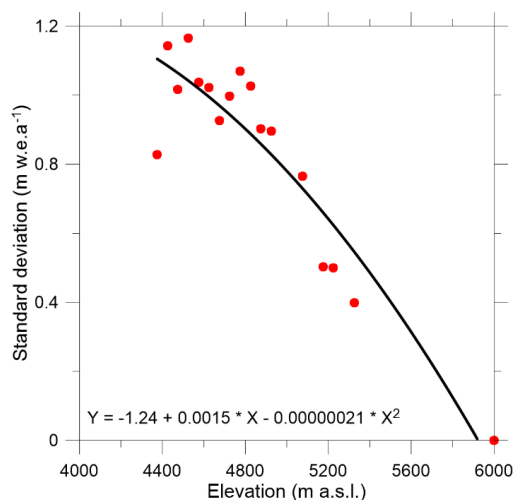
$$168 \quad b_{i,t} = \alpha_i + \beta_t \gamma_i + \varepsilon_{i,t}, \quad 2$$

169 where α_i , the spatial effects at location i , is the average point MB at the site over the whole
170 study period, β_t is the annual deviation from the average point MB (thus $\sum \beta_t = 0$), and $\gamma_i =$
171 σ_i / σ_{max} is a scaling factor defined as the ratio of the standard deviation of annual MB at site i
172 by the maximum standard deviation (σ_{max}) observed from the point MB measurements over a
173 long period. The $\varepsilon_{i,t}$ term represents residuals resulting from measurement errors and
174 inconsistencies between the model and observed data. The spatiotemporal decomposition
175 proposed in equation 2 assumes that β_t is the same at each location for any given year (t) and
176 thus has a glacier-wide significance while γ_i term accounts for nonlinear effects with elevation
177 (Vincent et al., 2018).

178 To compute the scaling factor, γ_i , on Chhota Shigri Glacier, standard deviations were
179 computed from the point MBs available for each 50-m elevation band as the point MBs are not
180 available each year from the same fixed locations (Fig. 2). The standard deviations were



181 computed only for 50-m elevation bands where mean annual MBs were available from in-situ
182 measurements over minimum ten years, and it was assumed that the computed standard
183 deviations are representative of the whole period of investigation (2002-2023). This resulted in
184 16 standard deviation values over the whole glacier with a maximum standard deviation of 1.17
185 m w.e. a⁻¹ at 4525 m a.s.l. (4500-4550 band) and a minimum standard deviation of 0.40 m w.e.
186 a⁻¹ at 5325 m a.s.l. The decreasing magnitude of standard deviation with elevation indicates
187 the decreasing sensitivity of the annual MB to temperature and precipitation (Fig. 2), as already
188 suggested by several studies on glaciers worldwide (Kuhn, 1984; Soruco et al., 2009; Basantes-
189 Serrano et al., 2016; Vincent et al., 2018; Wagon et al., 2021). The measurements are poor in
190 the accumulation area, and no measurement was available above 5325 m a.s.l.; therefore, after
191 some trials, we adjusted the standard deviation at 6000 m a.s.l. to be zero (Fig. 2). A decreasing
192 trend in standard deviation values below 4525 m a.s.l. (Fig. 2) is due to the presence of debris
193 cover over the tongue of Chhota Shigri Glacier (Fig. 1) that undermines the glacier's sensitivity
194 to climate (Vincent et al., 2013; Banerjee and Shankar, 2013). The scaling factor, γ_i , at each
195 point MB location, was computed from the 2-degree polynomial function, fitted over the
196 standard deviation vs elevation scatter plot (Fig. 2).



197

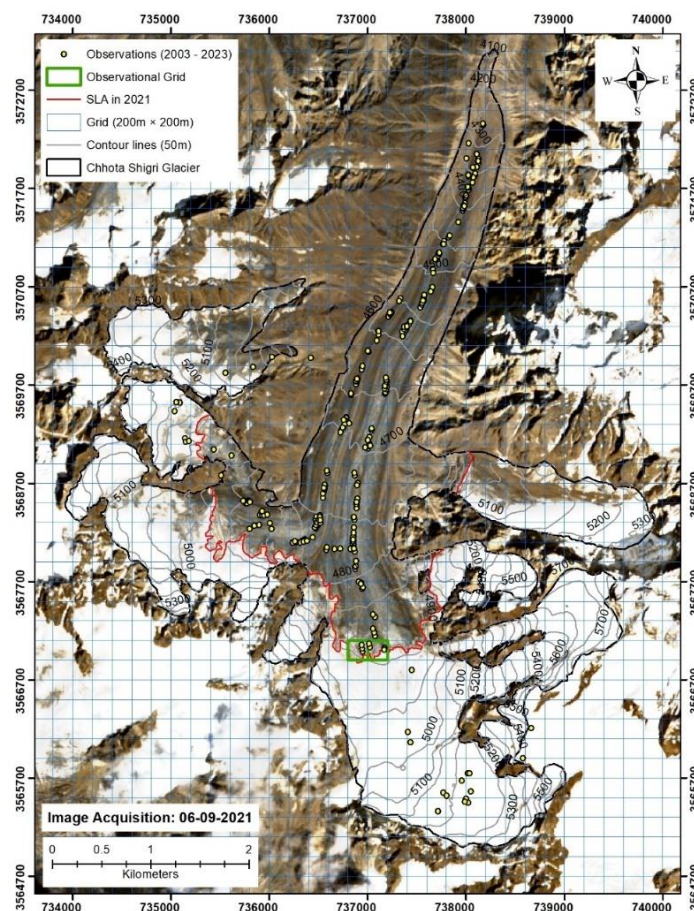
198 **Figure 2:** Standard deviations of the annual MBs versus elevation. The black line corresponds
199 to a polynomial fit (degree of freedom = 2). The standard deviations were estimated for those
200 50m elevation bands where a minimum of 10 years of point measurements were available at
201 each site, and it is assumed to be zero at 6000 m a.s.l. (above glacier top at 5830 m a.s.l.).
202

203 The nonlinear model was run at 200m x 200m spatial resolution over 2002-2023 using
204 all available point MBs (413-point measurements, excluding the erroneous measurements,



205 section 3.3) and polynomial equation (Fig. 2; details can be found in SI of Vincent et al., 2018).
206 The MB is assumed to be spatially constant over each 200m x 200m grid for a given year. If
207 there is more than one observation in a grid in a given year, then the mean MB of the available
208 observations was used for MB computation. The size of the grid is a compromise between the
209 spatial variability and the density of available point measurements.

210 Field measurements were unavailable in the 2020/21 year (section 3.1); hence, the
211 nonlinear model cannot be run. To run the model, at least one point MB measurement is
212 required each year (Vincent et al., 2018). We assumed the snow line altitude (SLA) at the end
213 of the ablation season to be equivalent to the equilibrium line altitude (ELA) (Rabatel et al.,
214 2005; Brun et al, 2015; Davaze et al., 2020; Barandun et al., 2021). The SLA was delineated
215 on 6 September 2021 Sentinel image and zero MBs (MB at ELA = 0 m w.e.) were assumed for
216 two 200m x 200m grids where MB observations were available from other years (Fig. 3). It is
217 to be noted that there was no other cloud-free image from September 2021. The MB estimation
218 from SLA using nonlinear model is discussed in detail in section 5.3.



219

220 **Figure 3:** Distribution of all 413-point MB measurements (yellow dots) available over 2002-
 221 2023 on Chhota Shigri Glacier. The grids (in light blue) show spatial resolution of 200m x
 222 200m of the nonlinear model. For 2020/21, no field measurement was conducted hence two-
 223 point MBs (grids shown with green colour outline), were selected
 224 on delineated SLA to run the model. The background is Sentinel image from 6 September 2021
 225 which is used to delineate the SLA.

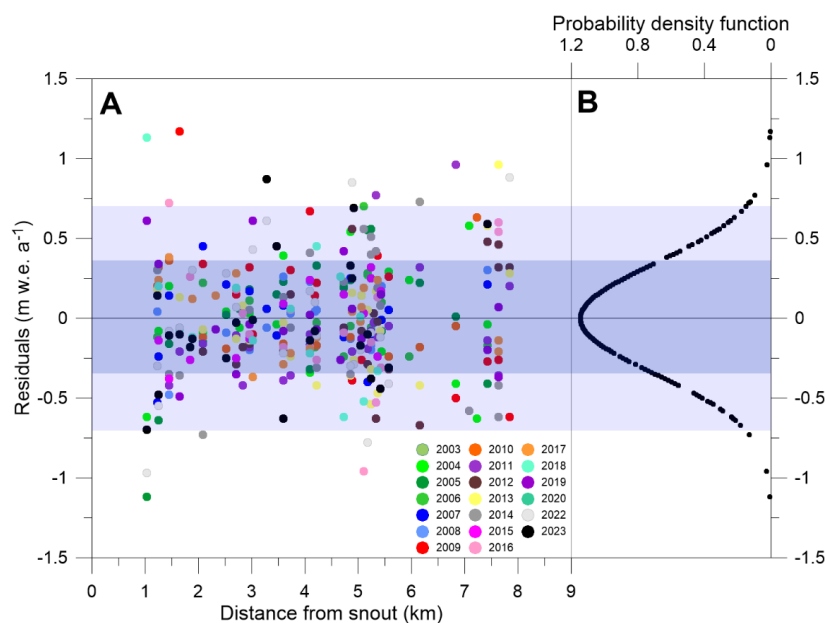
226 The model output provides the mean α_i and mean γ_i for each point location over 2002-
 227 2023, and β_t for each year (equation 2). The calculation of glacier-wide MB needs to get a
 228 spatial distribution of α_i over the whole surface area of the glacier. First, for each 50-m
 229 elevation range (e), mean α_e was estimated from all available α_i by taking a simple arithmetic
 230 mean and γ_e from all available γ_i from respective elevation bands (equation 2). The modelled
 231 point MBs were available over the 4355–5512 m a.s.l. elevation range and beyond this range,
 232 the mean α_e and γ_e from the lowest (4300–4350 m a.s.l.) and highest (5500–5550 m a.s.l.)
 233 ranges were used to cover the lowest (0.15 km²) and highest (0.68 km²) parts of the glacier.



234 Second, applying α_e , γ_e and β_l from all elevation bands in equation 1 along with corresponding
 235 elevation areas, the annual glacier-wide MBs over 2002-2023 were estimated.

236 3.3 Tracking the erroneous in-situ point mass balances

237 The nonlinear model computes the residuals (difference between the measured and theoretical
 238 values) of each measured point MB and can detect errors in in-situ point MB data (Vincent et
 239 al., 2018). The distribution of residuals over the glacier as a function of distance from the snout
 240 showed no spatio-temporal pattern (Fig. 4A), indicating that the nonlinear model does not
 241 provide any apparent bias for any specific year. As expected, the residuals followed a normal
 242 distribution with a standard deviation (STD) of 0.35 m w.e. a⁻¹ (Fig. 4B). To detect the
 243 measurement errors in the point MBs in the Chhota Shigri measurement network over 2002–
 244 2023, we assumed all the point MBs having residuals >2STD (0.70 m w.e. a⁻¹) to be suspicious.
 245 Of 423-point MB measurements, 15 such point MBs were found and investigated further. Five-
 246 point MBs had been wrongly reported from the notebooks and thus have been corrected. We
 247 could not find any reason for the rest of the suspicious points. Therefore, they have been
 248 considered wrong and discarded in the final model run. The wrong field measurements come
 249 from different years (five ablation point measurements from 2009, 2012, 2018 and 2022, and
 250 five accumulation point measurements from 2011, 2014 and 2022) (Fig. 4). The standard
 251 deviation of the residuals from the nonlinear model reduced from 0.35 to 0.30 m w.e. a⁻¹ after
 252 correction/removal of suspicious point MB measurements.



253



254 **Figure 4:** (A) Shows the residuals between measured and modelled point MBs from the
255 nonlinear model using all available 423-point MBs as a function of distance from glacier snout
256 for each hydrological year between 2002 and 2023. The dark and light blue shaded envelopes
257 represent the 1 STD and 2 STD values, respectively. (B) shows the probability density function
258 (normal distribution curve) of all point MB residuals between 2002 and 2023.

259

260 3.4 Areal changes and debris cover estimation

261 The areal changes and debris cover were estimated on Chhota Shigri, Sichum and Hamtah
262 glaciers by manual delineation following the Global Land Ice Measurements from Space
263 (GLIMS) guidelines from the available ASTER (08/10/2003) and Pléiades images (26/09/2014
264 and 12/09/2020) (Raup et al., 2007). We have preferred manual delineation as it was considered
265 the most accurate method for delineating glacier outlines (Stokes et al., 2007; Garg et al., 2017;
266 Shukla and Qadir, 2016). The ice divides were interpreted using the Pléiades Digital Elevation
267 model (DEM). The changes were estimated for the ablation area for 2014 and 2020, as the
268 changes in the accumulation area were insignificant. The generated glacier outlines (2003,
269 2014 and 2020) were used to estimate the glacier area changes during 2003–2020. The
270 uncertainties associated with the glacier area were calculated using the buffer method (Bolch
271 et al., 2010; Chand and Sharma, 2015). The buffer size was half the pixel value (Bolch et al.,
272 2010; Andreassen et al., 2022).

273 3.5 Geodetic mass balances

274 The geodetic MBs were estimated over two periods (2003–2014 and 2014–2020) for Chhota
275 Shigri, Sichum and Hamtah glaciers using satellite stereo images from ASTER (15 m
276 resolution) acquired on 08/10/2003 and Pléiades (0.70 m resolution) acquired on 26/09/2014
277 and 12/09/2020, respectively. The ASTER October 2003 stereo-pair was preferred to other
278 ASTER or SPOT5 stereo pairs acquired in late summer 2002, 2004, and 2005 because it
279 resulted in the smallest uncertainties. The stereo images were acquired close to the end of the
280 hydrological year, reducing the impact of any seasonal offset. The DEM generation, co-
281 registration and MB calculation procedure is the same as in Falaschi et al. (2023). Uncertainties
282 for the glacier-wide geodetic MB were estimated using the patch method (Wagnon et al.,
283 2021).

284 Geodetic MBs were estimated over 10.97 years (from 08/10/2003 to 26/09/2014) and
285 5.96 years (from 26/09/2014 to 12/09/2020) and linearly scaled to estimate the geodetic MBs
286 over 11- and 6-year periods, respectively to make a direct comparison with the in-situ MBs
287 (estimated from end of September to end of September next year). Further, the WT glacier



288 fragmented sometime around 2012 (Srivastava et al., 2022) and its geodetic MBs were
289 estimated with Chhota Shigri (area-weighted) (Table 1) for direct comparison with the
290 traditional and nonlinear MBs, including the WT glacier.

291 **3.6 Homogenization of glacier-wide mass balances**

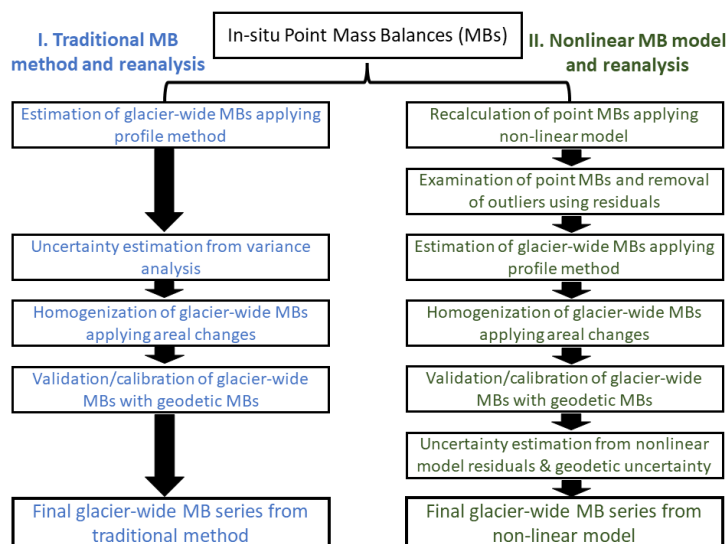
292 In initial studies (Wagon et al., 2007; Azam et al., 2012), a fixed hypsometry (glacier area and
293 elevation) from SPOT5 2005 DEM was used, while in follow-up studies (Azam et al., 2014;
294 Mandal et al., 2020) a fixed hypsometry from Pléiades August 2014 DEM was used to estimate
295 the traditional MBs on Chhota Shigri Glacier. These fixed hypsometries insert bias in the MB
296 series (Cogley et al., 2011; Zemp et al., 2013). Here, the Chhota Shigri Glacier annual MBs
297 (from the traditional method and nonlinear model) are homogenized with the linearly changing
298 annual hypsometries from ASTER and Pléiades DEMs over 2003–2014 and Pléiades DEMs
299 over 2014–2020 (section 4.1). We adopted the approach suggested by Zemp et al. (2013) that
300 assumes a linear area change over a record period (N years) and estimates the area (s) of an
301 elevation band (e) for each year (t) as follows:

302

$$303 \quad s_{e,t} = s_{e,0} + \frac{t}{N} \cdot (s_{e,N} - s_{e,0}), \quad (3)$$

304

305 where $s_{e,0}$ and $s_{e,N}$ are the elevation bin areas from the first and the second geodetic survey,
306 respectively, and the time t is zero in the year of the first survey. The homogenization process
307 of both traditional and nonlinear MB series changed the annual glacier-wide MBs at most by
308 0.02 m w.e., reflecting the negligible impact of areal changes over the 2003–2020 period on
309 Chhota Shigri Glacier (section 4.1). Post-2020, the hypsometry of the 2020 year was used to
310 estimate the MBs till 2023. Figure 5 summarizes the overall methodology step-by-step,
311 including homogenization, validation/calibration and error estimation (sections 3.7 and 3.9).



312

313 **Figure 5:** Conceptual diagram of the overall methodology: homogenization, uncertainty
 314 estimation, validation, and calibration steps.

315

316 3.7 Validation and calibration of glacier-wide mass balances

317 Previously, we validated the traditional MBs with geodetic MB available over 2005–2014
 318 (Azam et al., 2016). The systematic biases were within the uncertainty ranges of traditional and
 319 geodetic MBs; hence, no calibration was done. In this study, we repeated this validation over
 320 two periods when the geodetic MBs were calculated (section 4.2).

321 The traditional as well as nonlinear MBs over 2003–2014 were not statistically different
 322 from the geodetic MB, and the null hypothesis H_0 (the cumulative glaciological MB is not
 323 statistically different from the geodetic MB) was accepted at 95% and 90% levels (Zemp et al.,
 324 2013). However, over 2014–2020, both traditional and nonlinear MBs were statistically
 325 different from the geodetic MBs and the null hypothesis H_0 was rejected at 95% as well as 90%
 326 levels. This showed that the systematic biases were significant over 2014–2020 (Table 2). Even
 327 though we did not observe a significant bias over 2003–2014, we decided to calibrate the
 328 traditional as well as nonlinear MBs over both periods as suggested in previous studies (Thibert
 329 et al., 2008; Huss et al., 2009; Andreassen et al., 2016; Wagnon et al., 2021).

330 In the calibration procedure, the annual relative variability of glacier-wide MBs is taken
 331 from the MB series and the series was fitted to the multi-annual geodetic MB, B_g , as follows:



332
$$B_{a,cal} = B_a + \frac{(B_g - \sum_N B_a)}{N}, \quad (4)$$

333 where $B_{a,cal}$ is the annual calibrated glacier-wide MB and N is the number of years over which
334 the geodetic MB has been estimated. It should be mentioned that the MBs obtained from
335 traditional method or nonlinear model refer only to the surface MB, whereas the geodetic MBs
336 also integrate the internal and basal MBs, assumed to be small compared to the surface MB
337 (Cuffey and Paterson, 2010).

338 3.8 Calibration of mean altitudinal mass balances

339 The mean altitudinal MBs ($b_{e,t}$) for each 50-m elevation band (e) and each year (t) were
340 computed using equation 1 exploiting the values of α_i , β_t and γ_i obtained from the nonlinear
341 model. These altitudinal mean MBs were adjusted to fit the calibrated annual glacier-wide
342 MBs following Zemp et al. (2013). First, the centred mean altitudinal MB ($\beta_{e,t}$) is calculated
343 as the deviation from the uncalibrated annual nonlinear MBs (B_a):

344
$$\beta_{e,t} = b_{e,t} - B_a, \quad (5)$$

345 Then, the calibrated altitudinal mean MB ($b_{e,t,cal}$) for each year is estimated as:

346
$$b_{e,t,cal} = \beta_{e,t} + B_{a,cal}, \quad (6)$$

347 The equilibrium line altitude (ELA_{cal}) and MB gradient for each year (t) are also estimated by
348 plotting the linear regression over the calibrated annual mean altitudinal MBs ($b_{e,t,cal}$) over an
349 elevation range of 4375-5225 m. Finally, using the calibrated $ELAs$, the calibrated $AARs$ were
350 estimated each year (Table 3).

351 3.9 Random error estimation in nonlinear mass balances

352 The random error ($\sigma_{B_{n,cal}}$) in calibrated nonlinear glacier-wide MB is estimated following:

353
$$\sigma_{B_{n,cal}} = \pm \sqrt{\frac{\sigma_{B_g}^2}{N} + \sum s_i^2 \sigma_\varepsilon^2}, \quad (7)$$

354

355 σ_{B_g} is the error in the geodetic MBs ($\sigma_{B_g} = 0.57$ and 0.36 m w.e. a^{-1} over 2003–2014 and 2014–
356 2020, respectively), N is the number of years for geodetic MB estimation (section 3.3), s_i terms
357 represent the relative areas of each 50-m elevation band (except for 5400-5850 m a.s.l. range
358 that has been treated as a single band) compared to the total glacier area (therefore $\sum s_i = 1$),
359 and $\sigma_\varepsilon = 0.30$ m w.e. a^{-1} is the standard deviation of the residual term of equation (2) obtained
360 with the nonlinear model (section 3.2). Equation 7 is valid for the hydrological years within



361 calibration periods (2003–2014 and 2014–2020). The random errors in nonlinear glacier-wide
362 MBs for 2002/03 and 2020–2023 hydrological years were estimated following the procedure
363 described in Wagnon et al. (2021). The mean annual random error, $\sigma_{B_{n,cal}}$, of the calibrated
364 nonlinear glacier-wide MB was estimated to be ± 0.19 m w.e. a^{-1} over 2002–2023, with slightly
365 higher random errors for the years outside the calibration period (Table 3).

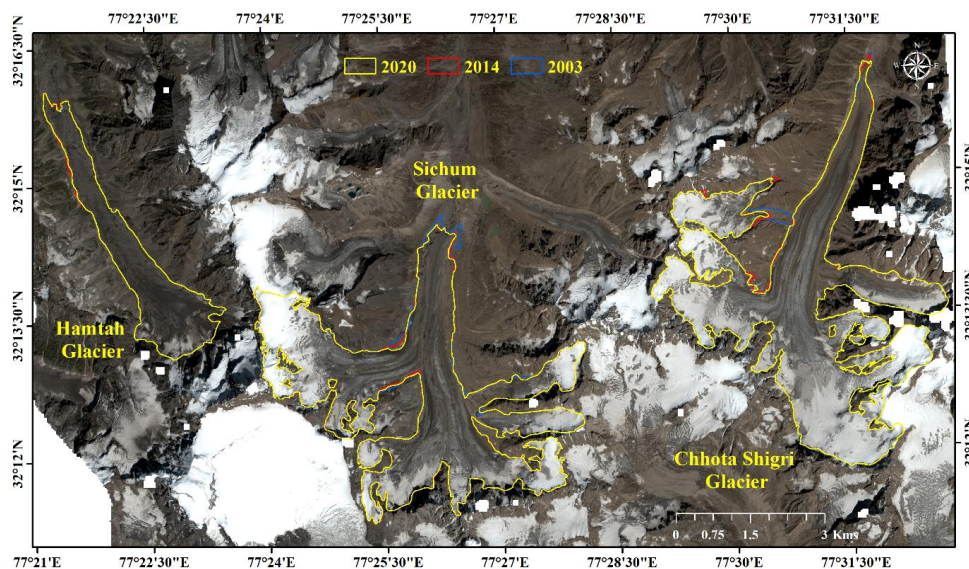
366 4. Results

367 4.1 Glacier area changes since 2003

368 Chhota Shigri, Sichum and Hamtah glaciers showed limited areal changes since 2003, mostly
369 restricted to the snout area (Table 1; Fig. 6). The estimated debris cover, corresponding to
370 September 2020 year, was 12%, 22% and 79% of the total area on Chhota Shigri, Sichum and
371 Hamtah glaciers, respectively (Table 1). During 2003–2020, the total area change for each
372 glacier was very small with a deglaciation rate of -0.07 ± 0.22 % a^{-1} , -0.07 ± 0.22 % a^{-1} and
373 -0.03 ± 0.19 % a^{-1} for Chhota, Sichum and Hamtah, respectively (Table 1).

374 4.2 Geodetic mass balances

375 The maps of elevation changes for 2003–2014 and 2014–2020 periods indicate a general
376 pattern of thinning for the glacier tongues and limited changes in the upper reaches of the
377 glaciers (Fig. 7). The area-weighted geodetic MB of Chhota Shigri Glacier (including WT) was
378 -0.43 ± 0.08 m w.e. a^{-1} over 2003–2020 (Table 1), with a higher annual wastage of $-0.51 \pm$
379 0.06 m w.e. a^{-1} over 2014–2020 compared to -0.38 ± 0.10 m w.e. a^{-1} over 2003–2014 (Table
380 2). Sichum and Hamtah glaciers showed slightly stronger annual mass wastage of -0.57 ± 0.08
381 and -0.51 ± 0.08 m w.e. a^{-1} , respectively over 2003–2020, with similarly an increased mass
382 wastage over the recent period (2014–2020) (Table 1). The slightly more negative glacier-wide
383 MBs on all these glaciers during 2014–2020 agree with a recent study suggesting an increased
384 wastage over the recent decade in the Himalaya (Hugonnet et al., 2021).



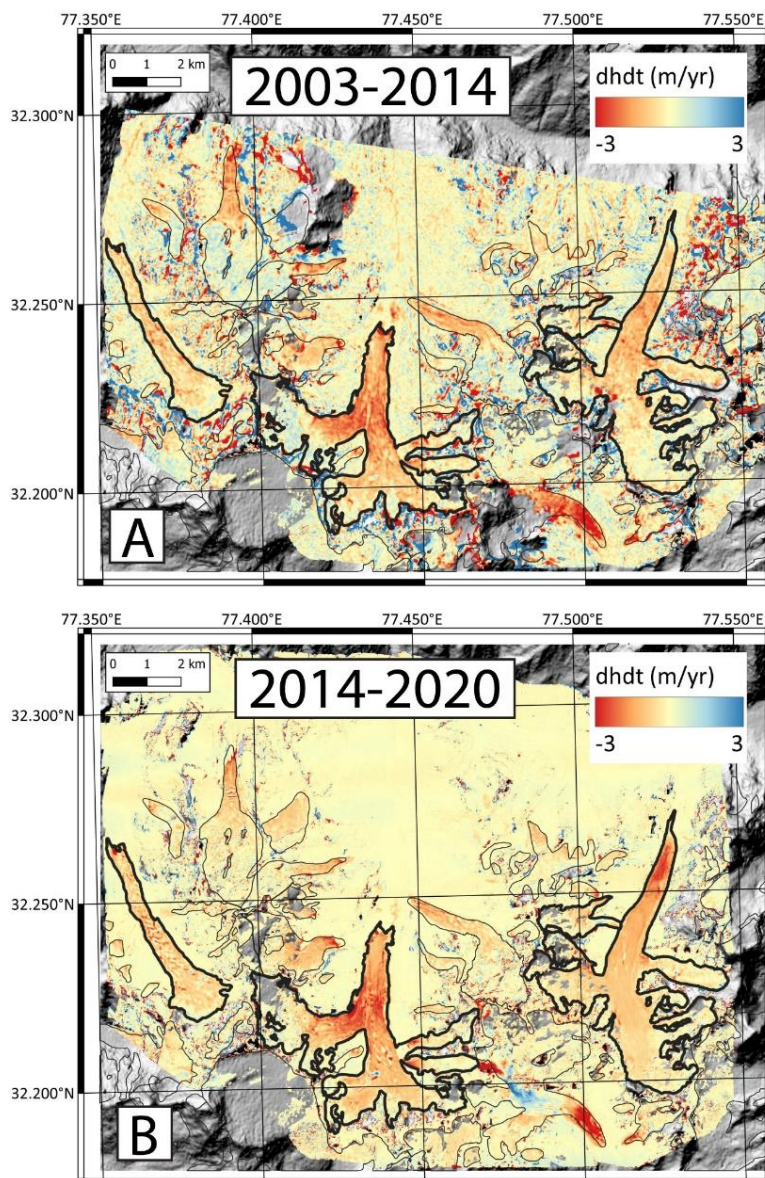
385

386 **Figure 6:** Glacier area change of Chhota Shigri, Sichum and Hamtah glaciers between 2003
 387 and 2020 (Background image is Pleiades satellite imagery of 12 September 2020; CNES 2020,
 388 Distribution Airbus D&S).

389

390 **Table 1:** The areal and geodetic mass changes on Chhota Shigri, Sichum and Hamtah glaciers
 391 over 2003-2014 and 2014-2020 periods.

Time Period	2003-14	2014-2020	2003-2020
Chhota Shigri with WT (Area = 15.47 km², 12% debris cover in 2020)			
Area change (km ²)	-0.15 ± 0.58	-0.05 ± 0.14	-0.20 ± 0.57
Area change rate (% a ⁻¹)	-0.09 ± 0.33	-0.05 ± 0.15	-0.07 ± 0.22
Geodetic MB (m w.e.)	-4.18 ± 0.57	-3.08 ± 0.36	-7.26 ± 0.93
Geodetic MB (m w.e. a ⁻¹)	-0.38 ± 0.10	-0.51 ± 0.06	-0.43 ± 0.08
Sichum (Area = 13.84 km², 22% debris cover in 2020)			
Area change (km ²)	-0.14 ± 0.52	-0.02 ± 0.12	-0.16 ± 0.52
Area change rate (% a ⁻¹)	-0.09 ± 0.34	-0.03 ± 0.14	-0.07 ± 0.22
Geodetic MB (m w.e.)	-6.07 ± 0.66	-3.68 ± 0.36	-9.75 ± 1.02
Geodetic MB (m w.e. a ⁻¹)	-0.55 ± 0.09	-0.61 ± 0.06	-0.57 ± 0.08
Hamtah (Area = 4.12 km², 79% debris cover in 2020)			
Area change (km ²)	-0.02 ± 0.13	-0.00 ± 0.03	-0.02 ± 0.13
Area change rate (% a ⁻¹)	-0.05 ± 0.29	-0.01 ± 0.13	-0.03 ± 0.19
Geodetic MB (m w.e.)	-5.19 ± 0.55	-3.44 ± 0.36	-8.63 ± 0.91
Geodetic MB (m w.e. a ⁻¹)	-0.47 ± 0.09	-0.57 ± 0.06	-0.51 ± 0.08



392

393 **Figure 7:** The thickness changes for Chhota Shigri, Sichum and Hamtah glaciers differencing
394 the ASTER 2003 (08/10/2003) and Pléiades (26/09/2014) DEMs over 2003–2014 and Pléiades
395 DEMs (26/09/2014 and 12/09/2020) over 2014–2020.

396 The mean annual geodetic mass wastage of -0.43 ± 0.08 m w.e. a^{-1} on Chhota Shigri
397 Glacier over 2003–2020 is in good agreement with the region-wide mean glacier mass wastage



398 of -0.37 ± 0.15 m w.e. a^{-1} over the whole Lahaul-Spiti region (glacierized area = 7960 km²)
 399 during a slightly different period (2000–2016), from multiple ASTER DEMs (Brun et al.,
 400 2017). Hence, Chhota Shigri is not only a reference glacier in the Himalaya (Azam, 2021) but
 401 also a representative glacier for the whole Lahaul-Spiti region, as already suggested (Vincent
 402 et al., 2013).

403 4.3 Annual and cumulative glacier-wide mass balances since 2002

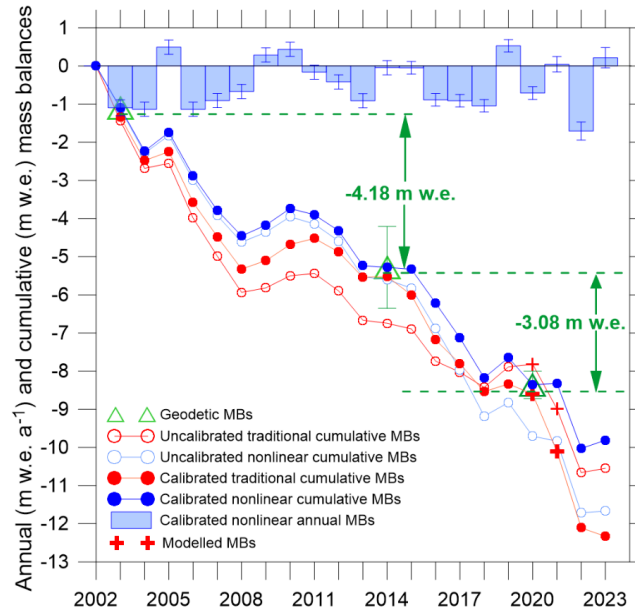
404 Table 2 and Fig. 8 show the traditional and nonlinear MBs (before and after calibration) and
 405 geodetic MBs over available periods. The traditional MBs were not available for 2019/20 and
 406 2020/21 (section 3.1); therefore, to calibrate these MBs and to cover the geodetic observations,
 407 the modelled MBs (2019/20 = 0.07 m w.e. and 2020/21 = -1.17 m w.e.) from surface energy
 408 balance approach (Srivastava and Azam, 2022b) were added to the series.

409 Compared to uncalibrated traditional MB series, uncalibrated nonlinear MB series
 410 showed much lesser biases with a slightly negative bias of -0.03 m w.e. a^{-1} (against a bias of
 411 -0.10 m w.e. a^{-1} in traditional MBs) over 2003–2014 and of -0.17 m w.e. a^{-1} (against a bias of
 412 0.33 m w.e. a^{-1} in traditional MBs) over 2014–2020 (Table 2; Fig. 8). Therefore, following
 413 equation 4, the nonlinear annual MBs were systematically increased by 0.03 m w.e. a^{-1} over
 414 2003–2014 and by 0.17 m w.e. a^{-1} over 2014–2020 while traditional MBs were systematically
 415 increased by 0.10 m w.e. a^{-1} over 2003–2014 and decreased by 0.33 m w.e. a^{-1} over 2014–
 416 2020 to match the geodetic estimates (Fig. 8). The hydrological years 2002/03 and 2020–2023
 417 are outside the calibration periods, but these years were also calibrated by the mean values of
 418 biases observed over 2003–2014 and 2014–2020, respectively. To avoid confusion, we
 419 discussed only the calibrated nonlinear glacier-wide MBs in the manuscript, although the
 420 calibrated traditional MBs are given in Table 2 and 3 for reference.

421 **Table 2:** Cumulative MBs (in parenthesis, mean annual MBs) from the traditional method,
 422 nonlinear model, and geodetic estimates over available periods. The balance year 2002/03 is
 423 not included here as it is not covered in the geodetic estimate available over 2003–2014. The
 424 cumulative traditional MB over the 2014–2020 period has been estimated by adding the
 425 modelled annual MB for 2019/20 (Srivastava and Azam, 2022b). All units are in m w.e. (m
 426 w.e. a^{-1}).

	2003–2014	2014–2019	2014–2020
Traditional MB	-5.31 (-0.48)	-1.14 (-0.23)	-1.07 (-0.18)*
Nonlinear MB	-4.48 (-0.41)	-3.22 (-0.64)	-4.10 (-0.68)
Geodetic MB	-4.18 (-0.38)	-	-3.08 (-0.51)
Calibrated traditional MB	-4.18 (-0.38)	-2.82 (-0.56)	-3.08 (-0.51)
Calibrated nonlinear MB	-4.18 (-0.38)	-2.37 (-0.47)	-3.08 (-0.51)

427 *estimated from traditional MBs (2014-2019) and modelled MB (2019/20).



428

429 **Figure 8:** Calibrated nonlinear annual glacier-wide MBs (with random errors) over 2002–
 430 2023, traditional cumulative MBs over 2002–2023, nonlinear cumulative MBs over 2002–
 431 2023, calibrated nonlinear cumulative MBs over 2002–2023, calibrated traditional cumulative
 432 MBs over 2002–2023, and geodetic MBs over 2003–2014 and 2014–2020 (with estimated
 433 uncertainties). The cumulative traditional MB series (2002–2019) is completed till 2023 by
 434 adding the modelled MB of 2019/2020 and 2020/21 from Srivastava and Azam (2022b).

435

436 **Table 3:** Calibrated nonlinear MBs ($B_{an,cal}$), calibrated traditional MBs ($B_{at,cal}$), MB gradients
 437 (db/dz), ELA_{cal} and AAR_{cal} on Chhota Shigri Glacier between 2002 and 2023.

Year	Glacier Area (km ²)	$B_{an,cal}$ (m w.e. a ⁻¹)	Error of $B_{an,cal}$ (m w.e. a ⁻¹)	$B_{at,cal}$ (m w.e. a ⁻¹)	db/dz (m w.e. (100) ⁻¹ a ⁻¹)	ELA_{cal} (m a.s.l.)	AAR_{cal} (%)	Difference $B_{an,cal} - B_{at,cal}$
2002/03	15.66	-1.10	0.21	-1.34	0.70	5145	33	0.24
2003/04	15.64	-1.14	0.19	-1.14	0.71	5156	32	0.01
2004/05	15.63	0.49	0.19	0.24	0.59	4911	67	0.26
2005/06	15.61	-1.14	0.19	-1.33	0.71	5157	32	0.19
2006/07	15.59	-0.91	0.19	-0.90	0.69	5128	36	-0.01
2007/08	15.57	-0.67	0.19	-0.84	0.67	5096	40	0.17
2008/09	15.56	0.29	0.19	0.22	0.60	4942	63	0.07
2009/10	15.54	0.43	0.19	0.42	0.59	4921	65	0.01
2010/11	15.52	-0.16	0.19	0.17	0.64	5022	50	-0.33
2011/12	15.50	-0.42	0.19	-0.36	0.66	5061	44	-0.06
2012/13	15.49	-0.91	0.19	-0.66	0.69	5131	34	-0.25
2013/14	15.47	-0.05	0.19	0.02	0.63	5004	53	-0.07
2014/15	15.46	-0.05	0.16	-0.48	0.64	5027	50	0.43
2015/16	15.45	-0.89	0.16	-1.18	0.70	5148	33	0.29
2016/17	15.44	-0.91	0.16	-0.62	0.70	5151	31	-0.29
2017/18	15.44	-1.05	0.16	-0.73	0.71	5167	30	-0.32
2018/19	15.43	0.53	0.16	0.21	0.60	4930	64	0.32
2019/20	15.42	-0.71	0.16	-0.26	0.69	5125	35	-0.45
2020/21	15.42	0.04	0.20	-1.49	0.63	5013	51	1.53
2021/22	15.42	-1.71	0.24	-2.00	0.76	5248	19	0.29
2022/23	15.42	0.21	0.27	-0.22	0.62	4985	56	0.44
Mean	15.51	-0.47	0.19	-0.58	0.66	5070	44	0.12
SD	0.08	0.65	0.02	0.67	0.05	97	14	0.42

438 *The calibrated traditional MBs for 2019/20 and 2020/21 years are originally from the model (Srivastava and Azam, 2022b).

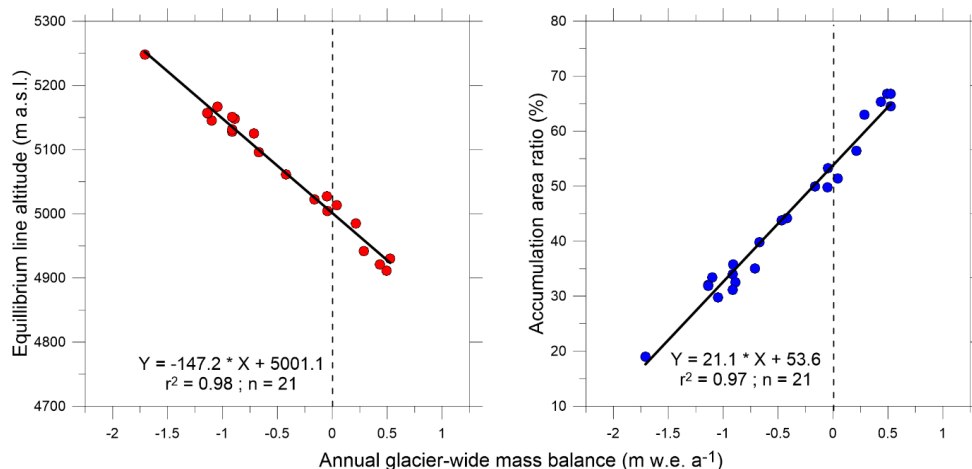


439 The annual calibrated glacier-wide MB from the nonlinear model varied from $0.53 \pm$
 440 $0.16 \text{ m w.e. a}^{-1}$ in 2018/19 to $-1.71 \pm 0.24 \text{ m w.e. a}^{-1}$ in 2021/22 with a standard deviation of
 441 $0.65 \text{ m w.e. a}^{-1}$ during 2002–2023 (Table 3). In the 21-year-long MB series, six hydrological
 442 years (2004/05, 2008/09, 2009/10, 2018/19, 2020/21, and 2022/23 showed positive/near steady
 443 state MBs. The mean annual glacier-wide MB was estimated to be $-0.47 \pm 0.19 \text{ m w.e. a}^{-1}$,
 444 equivalent to a cumulative loss of -9.81 m w.e. over 2002–2023 (Table 3).

445 4.4 Equilibrium line altitude and accumulation area ratio

446 Using the calibrated mean altitudinal MBs (section 3.8), the equilibrium line altitude ELA_{cal} ,
 447 accumulation area ratio AAR_{cal} and MB gradients (db/dz) were also estimated. The maximum
 448 ELA_{cal} was 5248 m a.s.l. corresponding to the most negative MB of $-1.71 \pm 0.24 \text{ m w.e. a}^{-1}$
 449 and minimum AAR_{cal} of 19% in 2021/22, while the minimum ELA_{cal} was 4911 m a.s.l.
 450 corresponding to a positive MB of $0.49 \pm 0.19 \text{ m w.e. a}^{-1}$ and a maximum AAR_{cal} of 67% in
 451 2004/05. The mean ELA_{cal} was 5070 m a.s.l. corresponding to a mean mass wastage of -0.47
 452 $\pm 0.19 \text{ m w.e. a}^{-1}$ and mean AAR_{cal} of 44% over 2002-2023.

453 The annual ELA_{cal} and AAR_{cal} showed good correlations with annual glacier-wide MBs
 454 ($r^2 = 0.98$ and 0.97 , respectively) over 2002-2023 (Fig. 5). The ELA_{cal} for a zero glacier-wide
 455 MB (ELA_0) was also computed from the regression between glacier-wide MBs and ELA_{cal} over
 456 2002-2023 and calculated as $\sim 5001 \text{ m a.s.l.}$ (Fig. 9). Similarly, AAR_0 was computed as $\sim 54\%$
 457 for steady-state glacier-wide MB.



458

459 **Figure 9:** The ELA and AAR as a function of annual glacier-wide MB.

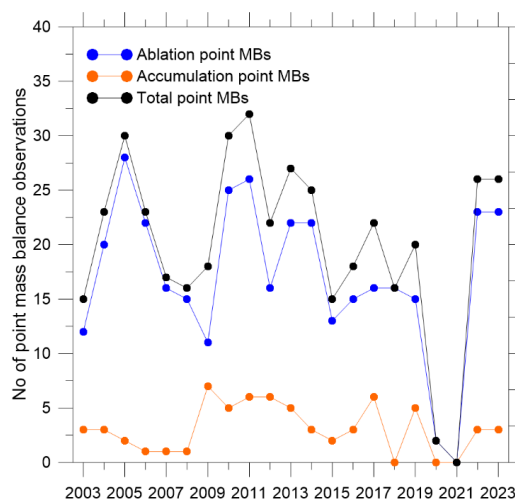
460



461 **5. Discussion**

462 **5.1 Biases in glacier-wide mass balances and performance of nonlinear model**

463 A total of 358 annual ablation and 65 annual accumulation point measurements were observed
 464 on Chhota Shigri Glacier over 2002–2023 to estimate the glacier-wide MBs (five ablation and
 465 five accumulation point MB measurements were removed before final model run; section 3.3).
 466 Figure 10 shows the temporal evolution of the number of these point measurements, and Table
 467 S1 provides the details about these point MBs. In general, the point MB measurement network
 468 (especially the accumulation points) has been poor after 2014 (section 3.1, Fig. 10). The eastern
 469 accumulation site at 5550 m a.s.l. (Fig. 1) could only be accessed five times (2003, 2004, 2005,
 470 2009, 2011) over the 2002-2023 period, while no accumulation measurements were done in
 471 2018, 2020 and 2021 (section 3.1). Occasionally, the ablation measurements were also missing
 472 due to missing stakes (heavy ablation or destroyed stakes). In the traditional method, these
 473 missing measurements were filled with extrapolated values from nearby ablation/accumulation
 474 MB measurements or previous years' point MB measurements to estimate the glacier-wide
 475 MBs (Azam et al., 2016; Mandal et al., 2020; Table S1).



476

477 **Figure 10:** Number of available ablation, accumulation, and total point MBs for each
 478 hydrological year between 2002 and 2023.

479 The systematic biases in glacier-wide annual MB series with the same monitoring
 480 network are expected to be of the same sign throughout the observation period, and the series
 481 is systematically adjusted to match the geodetic MBs available over one or more periods (Zemp
 482 et al., 2013; Wagnon et al., 2021). Nonlinear MB series on Chhota Shigri Glacier showed
 483 negative biases (−0.03 and −0.17 m w.e. a^{−1} over the 2003-2014 and 2014-2020 periods,



484 respectively), suggesting that the nonlinear model can reasonably estimate the glacier-wide
485 MBs with the existing monitoring network. Conversely, the traditional MB series showed a
486 negative bias (-0.10 m w.e. a^{-1}) over the 2003-2014 period and a large, positive bias (0.33 m
487 w.e. a^{-1}) over the 2014-2020 (Fig. 8; Table 2). The major disagreement between the cumulative
488 nonlinear and traditional MB curves after 2017 (Fig. 8) is likely due to a degradation of the
489 quality of field observations due to harsh weather, too short field surveys, or observers not
490 experienced enough (Fig. 10; Table S1; section 3.1).

491 To further investigate the performance of the nonlinear model compared to the traditional
492 MB method, we calibrated both the MB series with the geodetic MB estimated using ASTER
493 (08/10/2003) and Pléiades (12/09/2020) DEMs (details in SI) and used the geodetic MB over
494 2003–2014 (section 4.2) to validate both the calibrated series. The calibrated nonlinear MB
495 series showed a good agreement with the available geodetic MB (-3.88 m w.e. against -4.18
496 m w.e.), while the traditional MB showed very strong deviation from the geodetic MB over
497 2003–2014 (-6.13 m w.e. against -4.18 m w.e.) (Fig. S1). This good agreement between
498 nonlinear and geodetic MBs over 2003-2014 shows the robustness of the nonlinear model for
499 the glacier-wide mass balance estimation. Further, this comparison also highlights the
500 importance of using short-duration geodetic MB estimates for the calibration process, as with
501 two calibration periods; the calibrated traditional MB is in better agreement with the geodetic
502 MB (Fig. S1).

503 The nonlinear model shows a much better agreement with geodetic MBs than the
504 traditional method (Fig. 8; Table 2) mainly due to the (i) capability of the nonlinear model to
505 better capture the spatial variability of surface MB from a heterogeneous, discontinuous and
506 limited point MB data series than the traditional method (Vincent et al., 2018), (ii)
507 correction/exclusion of erroneous measurements (section 3.3) and (iii) exclusion of the
508 extrapolated ablation/accumulation points in the nonlinear model that might have introduced
509 biases in traditional MB. The outperformance of the nonlinear model suggests that the
510 extrapolation of point accumulations (in case of missing point measurements) in estimating the
511 glacier-wide MB using the traditional method is risky.

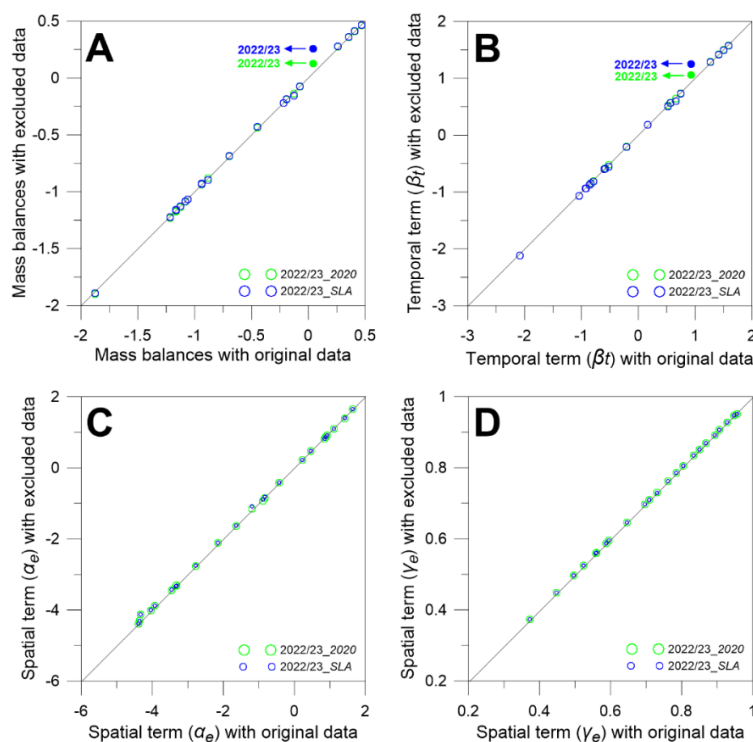
512 **5.2 2019/20 glacier-wide mass balance from two point mass balances**

513 The spatial and temporal terms in equation (2) are computed from a data sample available from
514 the whole series; therefore, MB computation is expected to be affected by missing data from
515 any single year (or, in general, from all years whenever data is missing). The glacier-wide MB



516 for 2019/20 was estimated using only two point MB observations (section 3.2; Table S1);
 517 therefore, it might have biases (Lliboutry, 1974; Vincent et al., 2018).

518 To investigate the additional error, we selected the year 2022/23 to test the performance
 519 of the nonlinear model. The 2022/23 year was selected because it is among the years with the
 520 maximum of point MB observations, and they were performed at their original locations. The
 521 nonlinear model was re-run over the 2002-2023 period, keeping only two point MB data (out
 522 of 26) for 2022/23 year corresponding to the locations of the two point MB measurements in
 523 2019/20. With only two point MBs, the glacier-wide MB for 2022/23 was recomputed to be
 524 0.13 m w.e. a⁻¹ against the original MB of 0.04 m w.e. a⁻¹ with a difference of 0.09 m w.e. a⁻¹,
 525 while all other year's glacier-wide MBs were changed by a maximum of ±0.01 m w.e. a⁻¹ (Fig.
 526 11A). As expected, the changes in the temporal term, β_t , having a glacier-wide significance,
 527 showed significant deviation from 0.93 to 1.06 m w.e. a⁻¹ for 2022/23 year, while for other
 528 years it changed by maximum up to ±0.04 m w.e. a⁻¹ (Fig. 11B). Conversely, the deviations in
 529 mean altitudinal spatial terms α_e and γ_e were very small (maximum up to ±0.06 m w.e. and
 530 ±0.005, respectively) (Fig. 11C, 11D). Therefore, the temporal term (β_t) in equation (2) mainly
 531 controls the annual glacier-wide MB and it is severely affected for the years when the in-situ
 532 MB monitoring is poor (for instance, 2019/20 year).



533



534 **Figure 11:** Glacier-wide MBs (A), temporal (β_t) (B) and spatial terms (α_e , and γ_e) (C and D,
535 **respectively**) obtained with the nonlinear model following two different scenarios as a function
536 of their original values obtained with full dataset. In the first scenario (2023/23_2020), we
537 remove all the data from 2022/23 (24-point MBs) except two located at the observation points
538 in 2019/20 (see section 5.2). In the second scenario (2022/23_SLA), we remove all the data
539 from 2022/23 and keep only two point MB data (= 0 m w.e.) obtained along the SLA (see
540 section 5.3). The filled dots highlight the test year of 2022/23.

541 The deviation of 0.09 m w.e. a^{-1} in glacier-wide MB estimated with only two point
542 MBs is less than the estimated random error of 0.27 m w.e. a^{-1} in 2022/23 glacier-wide MB in
543 original model run; therefore, it is assumed that the error in 2019/20 glacier-wide MB due to
544 restricted number of MB measurements is also less than the estimated random error of 0.16 m
545 w.e. a^{-1} (Table 3). Unlike the traditional MB method, the nonlinear model can fill the gaps in
546 glacier-wide MB where some point MB observations are missing and can provide a consistent
547 series of temporal fluctuations.

548 5.3 2020/21 glacier-wide mass balance from nonlinear model-SLA method

549 The glacier-wide MB for 2020/21 year was estimated by inferring two point MB input from
550 end-of-summer SLA, assuming it to be equivalent to ELA (i.e., MB = 0 m w.e.) (section 3.2;
551 Fig. 3). Due to only two point MB input data, the modelled glacier-wide MB for 2020/21 may
552 also have additional errors.

553 To quantify this error, we repeated the same exercise as in section 5.2 for the year
554 2022/23, this time keeping again two point MB data of 2022/23, but at the two sites where
555 point MB data have been assessed to be zero in 2020/21. The resulting 2022/23 glacier-wide
556 MB is 0.26 m w.e. a^{-1} , 0.22 m w.e. a^{-1} higher than the original value (Fig. 11A), mainly
557 explained by the β_t term (Fig. 11B). This difference is still lower than the estimated random
558 error of 0.27 m w.e. a^{-1} in 2022/23 (Table 3). However, there are still possible biases in glacier-
559 wide MB of 2020/21 year as the SLA was delineated from a Sentinel image from 6 September
560 2021 (section 3.2; Fig. 3) that is not exactly from the end of ablation season (30 September) on
561 Chhota Shigri Glacier. The surface energy balance model estimated a MB of -0.19 m w.e. over
562 the 6 September – 30 September 2021 (Srivastava and Azam, 2022a). However, this seasonal
563 offset correction in SLA-derived annual MB may be given, but it was avoided as the differences
564 are within the estimated random error of 0.20 m w.e. a^{-1} (Table 3). Our analysis shows that the
565 glacier-wide MB can also be estimated from SLA using the nonlinear model if the field
566 measurements cannot be carried out for some specific years.



567 However, the nonlinear model-SLA method has several limitations: (i) the delineated
568 SLA must pass through grid/s having previous point MB observation/s (Fig. 3) as at least one
569 previous measurement is required to run the model, (ii) the delineated SLA must be from the
570 end of ablation season to consider it as ELA, (iii) SLA delineation has its challenges and often
571 it is difficult to find the cloud-free image for delineation at the end of ablation season (Brun et
572 al., 2015; Racoviteanu et al., 2019), and (iv) SLA is severely affected by recent snowfall hence
573 must be checked with in-situ precipitation data before using SLA in nonlinear model. This
574 latter point implies that the ELA can be inferred from the end-of-ablation-season SLA, which
575 is not always possible over glaciers, especially in monsoon-dominated regions (Brun et al.,
576 2015).

577 **Conclusions**

578 This work reanalyses glacier-wide MBs by combining the traditional reanalysis framework
579 (Zemp et al., 2013) and the nonlinear MB model (Vincent et al., 2018). Previously, the annual
580 glacier-wide MBs had been estimated on Chhota Shigri Glacier since 2002, applying the
581 traditional glaciological method using heterogeneous in-situ point MB measurements. The
582 heterogeneous measurement network does not always catch the large spatiotemporal variability
583 of point MBs; hence, the point MB-elevation relationship is insufficient to investigate the
584 changes in glacier-wide MBs. Therefore, we applied the nonlinear model to compute the
585 glacier-wide MBs of Chhota Shigri Glacier as it enables the computation of the glacier-wide
586 MB from a heterogeneous in-situ point MB network. The nonlinear model was used to detect
587 the measurement errors. Out of 423-point measurements, seven were corrected from field
588 notebooks, and ten were recognized as wrong observations and discarded before running the
589 final model.

590 ASTER and Pléiades DEMs were used to estimate the geodetic MBs over 2003–2014
591 and 2014–2020 that have been used to reanalyse the nonlinear MBs. Nonlinear MBs agreed
592 well with the geodetic estimates available over 2003–2014 and 2014–2020, unlike traditional
593 MBs that showed large differences, especially over the 2014–2020 period. The reanalysed
594 nonlinear MBs showed a large annual variability ranging from 0.53 ± 0.16 m w.e. a^{-1} in
595 2018/19 to -1.71 ± 0.24 m w.e. a^{-1} in 2021/22. The Chhota Shigri Glacier is imbalanced with
596 a mean mass wastage of -0.47 ± 0.19 m w.e. a^{-1} , equivalent to a cumulative loss of -9.81 m
597 w.e. over 2002–2023.

598 With the 21-year-long MB observations, the Chhota Shigri Glacier MB series is the
599 longest in the Himalaya. This work has enabled the data set to be extended, optimised, and



600 corrected to provide the best possible mass balance series for this benchmark glacier. We plan
601 to monitor this glacier over a long period, with repeated satellite image acquisitions by the
602 Pléiades Glacier Observatory to regularly validate/calibrate the glacier-wide MB, typically
603 every five years.

604 Our detailed analysis suggests that the nonlinear model performs better in calculating
605 the glacier-wide MB than the traditional method as (i) the nonlinear MBs are in much better
606 agreement with the geodetic MB estimates, (ii) it can detect erroneous measurements, (iii) it
607 provides better glacier-wide MBs than those of the traditional method when the observational
608 network is very limited, and (iv) glacier-wide MB can be computed using SLA if the ablation-
609 end SLA passes through a grid cell that contains point MB observations from previous years.
610 Therefore, the application of the nonlinear model is suggested on all monitored glaciers
611 whenever data is sufficient. It becomes even more relevant in the Himalaya, where data are
612 sometimes missing due to access issues. However, the estimated glacier-wide MBs may
613 contain systematic bias (arises from the distribution of point measurements over the glacier)
614 and, therefore, should be checked and, if necessary, reanalysed with geodetic estimates.

615 **Author contribution**

616 MFA, CV and PW conceptualized the study. MFA did the nonlinear model runs and analysed
617 the data with the help of CV and PW. SS estimated the areal changes, the snow line altitudes,
618 and MBs from the energy balance model. EB estimated the geodetic MBs. MFA wrote the
619 paper with inputs from all co-authors.

620 **Competing interests**

621 At least one of the (co-)authors is a member of the editorial board of The Cryosphere.

622 **Acknowledgements**

623 MFA acknowledges the research grants from ISRO under the RESPOND scheme
624 (ISRO/RES/4/690/21-22), SERB (CRG/2020/004877) and MoES
625 (MOES/PAMC/H&C/131/2019-PC-II). EB acknowledges support from the French Space
626 Agency (CNES). Pléiades stereo-imagery of September 2020 was obtained through the
627 Pléiades Glacier Observatory. The authors are grateful to DST-IFCPAR/CEFIPRA project
628 n°3900-W1 and the French Service d'Observation GLACIOCLIM sponsored by IRD, which
629 provided financial support to conduct field trips and equipment. Thanks to all scientists,
630 Adhikari Ji and porters involved in the previous research expeditions on Chhota Shigri Glacier
631 since 2002.



632 **References**

633 Andreassen, L. M., Elvehøy, H., Kjøllmoen, B., and Engeset, R. V.: Reanalysis of long-term
634 series of glaciological and geodetic mass balance for 10 Norwegian glaciers, *The Cryosphere*,
635 10, 535–552, <https://doi.org/10.5194/tc-10-535-2016>, 2016.

636 Andreassen, L. M., Nagy, T., Kjøllmoen, B., and Leigh, J. R.: An inventory of Norway's
637 glaciers and ice-marginal lakes from 2018–19 Sentinel-2 data, *Journal of Glaciology*, 68, 1085–
638 1106, <https://doi.org/10.1017/jog.2022.20>, 2022.

639 Azam, M. F.: Need of integrated monitoring on reference glacier catchments for future water
640 security in Himalaya, *Water Security*, 14, 100098,
641 <https://doi.org/10.1016/j.wasec.2021.100098>, 2021.

642 Azam, M. F., Wagnon, P., Ramanathan, A., Vincent, C., Sharma, P., Arnaud, Y., Linda, A.,
643 Pottakkal, J. G., Chevallier, P., Singh, V. B., and Berthier, E.: From balance to imbalance: a
644 shift in the dynamic behaviour of Chhota Shigri glacier, western Himalaya, India, *Journal of*
645 *Glaciology*, 58, 315–324, <https://doi.org/10.3189/2012JoG11J123>, 2012.

646 Azam, M. F., Wagnon, P., Vincent, C., Ramanathan, A., Linda, A., and Singh, V. B.:
647 Reconstruction of the annual mass balance of Chhota Shigri glacier, Western Himalaya, India,
648 since 1969, *Annals of Glaciology*, 55, 69–80, <https://doi.org/10.3189/2014AoG66A104>, 2014.

649 Azam, M. F., Ramanathan, A., Wagnon, P., Vincent, C., Linda, A., Berthier, E., Sharma, P.,
650 Mandal, A., Angchuk, T., Singh, V. B., and Pottakkal, J. G.: Meteorological conditions,
651 seasonal and annual mass balances of Chhota Shigri Glacier, western Himalaya, India, *Annals*
652 *of Glaciology*, 57, 328–338, <https://doi.org/10.3189/2016AoG71A570>, 2016.

653 Azam, M. F., Wagnon, P., Berthier, E., Vincent, C., Fujita, K., and Kargel, J. S.: Review of the
654 status and mass changes of Himalayan-Karakoram glaciers, *Journal of Glaciology*, 64, 61–74,
655 <https://doi.org/10.1017/jog.2017.86>, 2018.

656 Azam, M. F., Kargel, J. S., Shea, J. M., Nepal, S., Haritashya, U. K., Srivastava, S., Maussion,
657 F., Qazi, N., Chevallier, P., Dimri, A. P., Kulkarni, A. V., Cogley, J. G., and Bahuguna, I.:
658 Glaciohydrology of the Himalaya-Karakoram, *Science*, 373, eabf3668,
659 <https://doi.org/10.1126/science.abf3668>, 2021.

660 Banerjee, A. and Shankar, R.: On the response of Himalayan glaciers to climate change, *Journal*
661 *of Glaciology*, 59, 480–490, <https://doi.org/10.3189/2013JoG12J130>, 2013.



662 Barandun, M., Pohl, E., Naegeli, K., McNabb, R., Huss, M., Berthier, E., Saks, T., and Hoelzle,
663 M.: Hot Spots of Glacier Mass Balance Variability in Central Asia, *Geophysical Research*
664 *Letters*, 48, e2020GL092084, <https://doi.org/10.1029/2020GL092084>, 2021.

665 Basantes-Serrano, R., Rabatel, A., Francou, B., Vincent, C., Maisincho, L., Cáceres, B.,
666 Galarraga, R., and Alvarez, D.: Slight mass loss revealed by reanalyzing glacier mass-balance
667 observations on Glacier Antisana 15 α (inner tropics) during the 1995–2012 period, *Journal of*
668 *Glaciology*, 62, 124–136, <https://doi.org/10.1017/jog.2016.17>, 2016.

669 Berthier, E., Arnaud, Y., Kumar, R., Ahmad, S., Wagnon, P., and Chevallier, P.: Remote
670 sensing estimates of glacier mass balances in the Himachal Pradesh (Western Himalaya, India),
671 *Remote Sensing of Environment*, 108, 327–338, <https://doi.org/10.1016/j.rse.2006.11.017>,
672 2007.

673 Berthier, E., Floricioiu, D., Gardner, A. S., Gourmelen, N., Jakob, L., Paul, F., Treichler, D.,
674 Wouters, B., Belart, J. M. C., Dehecq, A., Dussailant, I., Hugonnet, R., Kaab, A. M., Krieger,
675 L., Pálsson, F., and Zemp, M.: Measuring Glacier Mass Changes from Space - A Review,
676 *Reports on Progress in Physics*, 86, 036801, <https://doi.org/10.1088/1361-6633/acaf8e>, 2023.

677 Bolch, T., Yao, T., Kang, S., Buchroithner, M. F., Scherer, D., Maussion, F., Huintjes, E., and
678 Schneider, C.: A glacier inventory for the western Nyainqentanglha Range and the Nam Co
679 Basin, Tibet, and glacier changes 1976–2009, *The Cryosphere*, 4, 419–433,
680 <https://doi.org/10.5194/tc-4-419-2010>, 2010.

681 Bolch, T., Shea, J. M., Liu, S., Azam, F. M., Gao, Y., Gruber, S., Immerzeel, W. W., Kulkarni,
682 A., Li, H., Tahir, A. A., Zhang, G., and Zhang, Y.: Status and Change of the Cryosphere in the
683 Extended Hindu Kush Himalaya Region, in: *The Hindu Kush Himalaya Assessment: Mountains, Climate Change, Sustainability and People*, edited by: Wester, P., Mishra, A.,
684 Mukherji, A., and Shrestha, A. B., Springer International Publishing, Cham, 209–255,
685 https://doi.org/10.1007/978-3-319-92288-1_7, 2019.

687 Brun, F., Berthier, E., Wagnon, P., Kääb, A., and Treichler, D.: A spatially resolved estimate
688 of High Mountain Asia glacier mass balances from 2000 to 2016, *Nature Geosci*, 10, 668–673,
689 <https://doi.org/10.1038/ngeo2999>, 2017.

690 Brun, F., Dumont, M., Wagnon, P., Berthier, E., Azam, M. F., Shea, J. M., Sirguey, P., Rabatel,
691 A., and Ramanathan, Al.: Seasonal changes in surface albedo of Himalayan glaciers from



692 MODIS data and links with the annual mass balance, *The Cryosphere*, 9, 341–355,
693 <https://doi.org/10.5194/tc-9-341-2015>, 2015.

694 Chand, P. and Sharma, M. C.: Frontal changes in the Manimahesh and Tal Glaciers in the Ravi
695 basin, Himachal Pradesh, northwestern Himalaya (India), between 1971 and 2013,
696 *International Journal of Remote Sensing*, 36, 4095–4113,
697 <https://doi.org/10.1080/01431161.2015.1074300>, 2015.

698 Cogley, J., Hock, R., Rasmussen, L., Arendt, A., Bauder, A., Braithwaite, R., Jansson, P.,
699 Kaser, G., Möller, M., Nicholson, L., and Zemp, M.: Glossary of glacier mass balance and
700 related terms, <https://doi.org/10.5167/uzh-53475>, 2011.

701 Cogley, J. G.: Geodetic and direct mass-balance measurements: comparison and joint analysis,
702 *Annals of Glaciology*, 50, 96–100, <https://doi.org/10.3189/172756409787769744>, 2009.

703 Cuffey, K. M. and Paterson, W. S. B.: *The Physics of Glaciers*, Academic Press, 721 pp., 2010.

704 Davaze, L., Rabatel, A., Dufour, A., Hugonnet, R., and Arnaud, Y.: Region-wide annual glacier
705 surface mass balance for the European Alps from 2000 to 2016, *Frontiers in Earth Science*, 8,
706 149, <https://doi.org/10.3389/feart.2020.00149>, 2020.

707 Falaschi, D., Bhattacharya, A., Guillet, G., Huang, L., King, O., Mukherjee, K., Rastner, P.,
708 Yao, T., and Bolch, T.: Annual to seasonal glacier mass balance in High Mountain Asia derived
709 from Pléiades stereo images: examples from the Pamir and the Tibetan Plateau, *The*
710 *Cryosphere*, 17, 5435–5458, <https://doi.org/10.5194/tc-17-5435-2023>, 2023.

711 Funk, M., Morelli, R., and Stahel, W.: Mass balance of Griesgletscher 1961-1994: Different
712 methods of determination, *Massenbilanz des Griesgletschers 1961-1994: Verschiedene*
713 *Bestimmungsverfahren*, 33, 41–56, 1997.

714 Gantayat, P. and Ramsankaran, R.: Modelling evolution of a large, glacier-fed lake in the
715 Western Indian Himalaya, *Sci Rep*, 13, 1840, <https://doi.org/10.1038/s41598-023-28144-8>,
716 2023.

717 Gardner, A., Moholdt, G., Cogley, J., Wouters, B., Arendt, A., Wahr, J., Berthier, E., Hock, R.,
718 Pfeffer, W., Kaser, G., Ligtenberg, S., Bolch, T., Sharp, M., Hagen, J., Van den Broeke, M.,
719 and Paul, F.: A Reconciled Estimate of Glacier Contributions to Sea Level Rise: 2003 to 2009,
720 *Science (New York, N.Y.)*, 340, 852–857, <https://doi.org/10.1126/science.1234532>, 2013.



- 721 Garg, P. K., Shukla, A., and Jasrotia, A. S.: Influence of topography on glacier changes in the
722 central Himalaya, India, *Global and Planetary Change*, 155, 196–212,
723 <https://doi.org/10.1016/j.gloplacha.2017.07.007>, 2017.
- 724 Haq, M. A., Azam, M.F., Vincent, C.: Efficiency of artificial neural networks for glacier ice-
725 thickness estimation: a case study in western Himalaya, India. *Journal of Glaciology* 67(264),
726 671–684, <https://doi.org/10.1017/jog.2021.19>, 2021.
- 727
728 Harrison, S., Kargel, J. S., Huggel, C., Reynolds, J., Shugar, D. H., Betts, R. A., Emmer, A.,
729 Glasser, N., Haritashya, U. K., Klimeš, J., Reinhardt, L., Schaub, Y., Wiltshire, A., Regmi, D.,
730 and Vilímek, V.: Climate change and the global pattern of moraine-dammed glacial lake
731 outburst floods, *The Cryosphere*, 12, 1195–1209, <https://doi.org/10.5194/tc-12-1195-2018>,
732 2018.
- 733 Hugonnet, R., McNabb, R., Berthier, E., Menounos, B., Nuth, C., Girod, L., Farinotti, D., Huss,
734 M., Dussaillant, I., Brun, F., and Kääb, A.: Accelerated global glacier mass loss in the early
735 twenty-first century, *Nature*, 592, 726–731, <https://doi.org/10.1038/s41586-021-03436-z>,
736 2021.
- 737 Huss, M., Bauder, A., and Funk, M.: Homogenization of long-term mass-balance time series,
738 *Annals of Glaciology*, 50, 198–206, <https://doi.org/10.3189/172756409787769627>, 2009.
- 739 Jackson, M., Azam, M. F., Baral, P., Benestad, R., Brun, F., Muhammad, S., Pradhananga, S.,
740 Shrestha, F., Steiner, J. F., and Thapa, A.: Chapter 2: Consequences of climate change for the
741 cryosphere in the Hindu Kush Himalaya, <https://doi.org/10.53055/ICIMOD.1030>, 2023.
- 742 Kuhn, M.: Mass Budget Imbalances as Criterion for a Climatic Classification of Glaciers,
743 *Geografiska Annaler. Series A, Physical Geography*, 66, 229–238,
744 <https://doi.org/10.2307/520696>, 1984.
- 745 Kumar, A., Verma, A., Gokhale, A., Bhambri, R., Misra, A., Sundriyal, S., Dobhal, D., and
746 kishore, N.: Hydrometeorological assessments and suspended sediment delivery from a central
747 Himalayan glacier in the upper Ganga basin, *International Journal of Sediment Research*, 33,
748 <https://doi.org/10.1016/j.ijsrc.2018.03.004>, 2018.
- 749 Laha, S., Kumari, R., Singh, S., Mishra, A., Sharma, T., Banerjee, A., Nainwal, H. C., and
750 Shankar, R.: Evaluating the contribution of avalanching to the mass balance of Himalayan
751 glaciers, *Annals of Glaciology*, 58, 110–118, <https://doi.org/10.1017/aog.2017.27>, 2017.



- 752 Lliboutry, L.: Multivariate Statistical Analysis of Glacier Annual Balances, *Journal of*
753 *Glaciology*, 13, 371–392, <https://doi.org/10.3189/S0022143000023169>, 1974.
- 754 Mandal, A., Ramanathan, A., Azam, M. F., Angchuk, T., Soheb, M., Kumar, N., Pottakkal, J.
755 G., Vatsal, S., Mishra, S., and Singh, V. B.: Understanding the interrelationships among mass
756 balance, meteorology, discharge and surface velocity on Chhota Shigri Glacier over 2002–
757 2019 using in situ measurements, *Journal of Glaciology*, 66, 727–741,
758 <https://doi.org/10.1017/jog.2020.42>, 2020.
- 759 Mandal, A., Angchuk, T., Azam, M. F., Ramanathan, A., Wagnon, P., Soheb, M., and Singh,
760 C.: An 11-year record of wintertime snow-surface energy balance and sublimation at
761 4863 m a.s.l. on the Chhota Shigri Glacier moraine (western Himalaya, India), *The Cryosphere*,
762 16, 3775–3799, <https://doi.org/10.5194/tc-16-3775-2022>, 2022.
- 763 Miles, E., McCarthy, M., Dehecq, A., Kneib, M., Fugger, S., and Pellicciotti, F.: Health and
764 sustainability of glaciers in High Mountain Asia, *Nat Commun*, 12, 2868,
765 <https://doi.org/10.1038/s41467-021-23073-4>, 2021.
- 766 Mukherjee, K., Bhattacharya, A., Pieczonka, T., Ghosh, S., and Bolch, T.: Glacier mass budget
767 and climate reanalysis data indicate a climatic shift around 2000 in Lahaul-Spiti, western
768 Himalaya, *Climatic Change*, 148, 219–233, <https://doi.org/10.1007/s10584-018-2185-3>, 2018.
- 769 Nepal, S., Steiner, J. F., Allen, S., Azam, M. F., Bhuchar, S., Biemans, H., Dhakal, M., Khanal,
770 S., Li, D., Lutz, A., Pradhananga, S., Ritzema, R., Stoffel, M., and Stuart-Smith, R.: Chapter
771 3: Consequences of cryospheric change for water resources and hazards in the Hindu Kush
772 Himalaya, <https://doi.org/10.53055/ICIMOD.1031>, 2023.
- 773 Oerlemans, J.: *Glaciers and Climate Change*, CRC Press, 168 pp., 2001.
- 774 Østrem, G. and Stanley, A.: *Glacier mass balance measurements: a manual for field and office*
775 *work*. 1969.
- 776 Østrem, G. and Brugman, M.: *Glacier mass-balance measurements: a manual for field and*
777 *office work*, 1991.
- 778 Rabatel, A., Dedieu, J.-P., and Vincent, C.: Using remote-sensing data to determine
779 equilibrium-line altitude and mass-balance time series: validation on three French glaciers,
780 1994–2002, *Journal of Glaciology*, 51, 539–546,
781 <https://doi.org/10.3189/172756505781829106>, 2005.



- 782 Racoviteanu, A. E., Rittger, K., and Armstrong, R.: An automated approach for estimating
783 snowline altitudes in the Karakoram and eastern Himalaya from remote sensing, *Frontiers in*
784 *Earth Science*, 7, 220, <https://doi.org/10.3389/feart.2019.00220>, 2019.
- 785 Ramsankaran, R., Pandit, A., and Azam, M. F.: Spatially distributed ice-thickness modelling
786 for Chhota Shigri Glacier in western Himalayas, India, *International Journal of Remote*
787 *Sensing*, 39, 3320–3343, <https://doi.org/10.1080/01431161.2018.1441563>, 2018.
- 788 Raup, B., Racoviteanu, A., Khalsa, S. J. S., Helm, C., Armstrong, R., and Arnaud, Y.: The
789 GLIMS geospatial glacier database: A new tool for studying glacier change, *Global and*
790 *Planetary Change*, 56, 101–110, <https://doi.org/10.1016/j.gloplacha.2006.07.018>, 2007.
- 791 Rounce, D. R., Hock, R., Maussion, F., Hugonnet, R., Kochtitzky, W., Huss, M., Berthier, E.,
792 Brinkerhoff, D., Compagno, L., Copland, L., Farinotti, D., Menounos, B., and McNabb, R. W.:
793 Global glacier change in the 21st century: Every increase in temperature matters, *Science*, 379,
794 78–83, <https://doi.org/10.1126/science.abo1324>, 2023.
- 795 Shean, D. E., Bhushan, S., Montesano, P., Rounce, D. R., Arendt, A., and Osmanoglu, B.: A
796 Systematic, Regional Assessment of High Mountain Asia Glacier Mass Balance, *Frontiers in*
797 *Earth Science*, 7, <https://doi.org/10.3389/feart.2019.00363>, 2020.
- 798 Shugar, D. H., Jacquemart, M., Shean, D., Bhushan, S., Upadhyay, K., Sattar, A., Schwanghart,
799 W., McBride, S., De Vries, M. V. W., Mergili, M., Emmer, A., Deschamps-Berger, C.,
800 McDonnell, M., Bhambri, R., Allen, S., Berthier, E., Carrivick, J. L., Clague, J. J., Dokukin,
801 M., Dunning, S. A., Frey, H., Gascoïn, S., Haritashya, U. K., Huggel, C., Kääb, A., Kargel, J.
802 S., Kavanaugh, J. L., Lacroix, P., Petley, D., Rupper, S., Azam, M. F., Cook, S. J., Dimri, A.
803 P., Eriksson, M., Farinotti, D., Fiddes, J., Gnyawali, K. R., Harrison, S., Jha, M., Koppes, M.,
804 Kumar, A., Leinss, S., Majeed, U., Mal, S., Muhuri, A., Noetzli, J., Paul, F., Rashid, I., Sain,
805 K., Steiner, J., Ugalde, F., Watson, C. S., and Westoby, M. J.: A massive rock and ice avalanche
806 caused the 2021 disaster at Chamoli, Indian Himalaya, *Science*, 373, 300–306,
807 <https://doi.org/10.1126/science.abh4455>, 2021.
- 808 Shukla, A. and Qadir, J.: Differential response of glaciers with varying debris cover extent:
809 evidence from changing glacier parameters, *International Journal of Remote Sensing*, 37,
810 2453–2479, <https://doi.org/10.1080/01431161.2016.1176272>, 2016.



- 811 Shukla, A., Garg, P. K., and Srivastava, S.: Evolution of Glacial and High-Altitude Lakes in
812 the Sikkim, Eastern Himalaya Over the Past Four Decades (1975–2017), *Front. Environ. Sci.*,
813 6, 81, <https://doi.org/10.3389/fenvs.2018.00081>, 2018.
- 814 Soruco, A., Vincent, C., Francou, B., Ribstein, P., Berger, T., Sicart, J. E., Wagnon, P., Arnaud,
815 Y., Favier, V., and Lejeune, Y.: Mass Balance of Glaciar Zongo, Bolivia, between 1956 and
816 2006, using glaciological, hydrological and geodetic methods, *Annals of Glaciology*, 50, 1–8,
817 <https://doi.org/10.3189/172756409787769799>, 2009.
- 818 Srivastava, S. and Azam, M. F.: Mass- and Energy-Balance Modeling and Sublimation Losses
819 on Dokriani Bamak and Chhota Shigri Glaciers in Himalaya Since 1979, *Frontiers in Water*,
820 4, 874240, <https://doi.org/10.3389/frwa.2022.874240>, 2022a.
- 821 Srivastava, S. and Azam, Mohd. F.: Functioning of glacierized catchments in Monsoon and
822 Alpine regimes of Himalaya, *Journal of Hydrology*, 609, 127671,
823 <https://doi.org/10.1016/j.jhydrol.2022.127671>, 2022b.
- 824 Srivastava, S., Garg, P. K., and Azam, Mohd. F.: Seven Decades of Dimensional and Mass
825 Balance Changes on Dokriani Bamak and Chhota Shigri Glaciers, Indian Himalaya, Using
826 Satellite Data and Modelling, *J Indian Soc Remote Sens*, 50, 37–54,
827 <https://doi.org/10.1007/s12524-021-01455-x>, 2022.
- 828 Stokes, C. R., Clark, C. D., Lian, O. B., and Tulaczyk, S.: Ice stream sticky spots: A review of
829 their identification and influence beneath contemporary and palaeo-ice streams, *Earth-Science*
830 *Reviews*, 81, 217–249, <https://doi.org/10.1016/j.earscirev.2007.01.002>, 2007.
- 831 Thibert, E., Blanc, R., Vincent, C., and Eckert, N.: Glaciological and volumetric mass-balance
832 measurements: error analysis over 51 years for Glacier de Sarennes, French Alps, *Journal of*
833 *Glaciology*, 54, 522–532, <https://doi.org/10.3189/002214308785837093>, 2008.
- 834 Vincent, C., Ramanathan, A., Wagnon, P., Dobhal, D. P., Linda, A., Berthier, E., Sharma, P.,
835 Arnaud, Y., Azam, M. F., Jose, P. G., and Gardelle, J.: Balanced conditions or slight mass gain
836 of glaciers in the Lahaul and Spiti region (northern India, Himalaya) during the nineties
837 preceded recent mass loss, *The Cryosphere*, 7, 569–582, [https://doi.org/10.5194/tc-7-569-](https://doi.org/10.5194/tc-7-569-2013)
838 [2013](https://doi.org/10.5194/tc-7-569-2013), 2013.
- 839 Vincent, C., Soruco, A., Azam, M. F., Basantes-Serrano, R., Jackson, M., Kjølmoen, B.,
840 Thibert, E., Wagnon, P., Six, D., Rabatel, A., Ramanathan, A., Berthier, E., Cusicanqui, D.,



- 841 Vincent, P., and Mandal, A.: A Nonlinear Statistical Model for Extracting a Climatic Signal
842 From Glacier Mass Balance Measurements, *Journal of Geophysical Research: Earth Surface*,
843 123, 2228–2242, <https://doi.org/10.1029/2018JF004702>, 2018.
- 844 Vishwakarma, B. D., Ramsankaran, R., Azam, M. F., Bolch, T., Mandal, A., Srivastava, S.,
845 Kumar, P., Sahu, R., Navinkumar, P. J., Tanniru, S. R., Javed, A., Soheb, M., Dimri, A. P.,
846 Yadav, M., Devaraju, B., Chinnasamy, P., Reddy, M. J., Murugesan, G. P., Arora, M., Jain, S.
847 K., Ojha, C. S. P., Harrison, S., and Bamber, J.: Challenges in understanding the variability of
848 the cryosphere in the Himalaya and its impact on regional water resources,
849 <https://doi.org/10.3389/frwa.2022.909246>, 2022.
- 850 Wagon, P., Linda, A., Arnaud, Y., Kumar, R., Sharma, P., Vincent, C., Pottakkal, J. G.,
851 Berthier, E., Ramanathan, A., Hasnain, S. I., and Chevallier, P.: Four years of mass balance on
852 Chhota Shigri Glacier, Himachal Pradesh, India, a new benchmark glacier in the western
853 Himalaya, *J. Glaciol.*, 53, 603–611, <https://doi.org/10.3189/002214307784409306>, 2007.
- 854 Wagon, P., Brun, F., Khadka, A., Berthier, E., Shrestha, D., Vincent, C., Arnaud, Y., Six, D.,
855 Dehecq, A., Ménégoz, M., and Jomelli, V.: Reanalysing the 2007–19 glaciological mass-
856 balance series of Mera Glacier, Nepal, Central Himalaya, using geodetic mass balance, *Journal*
857 *of Glaciology*, 67, 117–125, <https://doi.org/10.1017/jog.2020.88>, 2021.
- 858 Yao, J., Chen, Y., Guan, X., Zhao, Y., Chen, J., and Mao, W.: Recent climate and hydrological
859 changes in a mountain–basin system in Xinjiang, China, *Earth-Science Reviews*, 226, 103957,
860 <https://doi.org/10.1016/j.earscirev.2022.103957>, 2022.
- 861 Zemp, M., Thibert, E., Huss, M., Stumm, D., Rolstad Denby, C., Nuth, C., Nussbaumer, S. U.,
862 Moholdt, G., Mercer, A., Mayer, C., Joerg, P. C., Jansson, P., Hynek, B., Fischer, A., Escher-
863 Vetter, H., Elvehøy, H., and Andreassen, L. M.: Reanalysing glacier mass balance
864 measurement series, *The Cryosphere*, 7, 1227–1245, <https://doi.org/10.5194/tc-7-1227-2013>,
865 2013.
- 866 Zemp, M., Frey, H., Gärtner-Roer, I., Nussbaumer, S. U., Hoelzle, M., Paul, F., Haeberli, W.,
867 Denzinger, F., Ahlstrøm, A. P., Anderson, B., Bajracharya, S., Baroni, C., Braun, L. N.,
868 Cáceres, B. E., Casassa, G., Cobos, G., Dávila, L. R., Granados, H. D., Demuth, M. N., Espizua,
869 L., Fischer, A., Fujita, K., Gadek, B., Ghazanfar, A., Hagen, J. O., Holmlund, P., Karimi, N.,
870 Li, Z., Pelto, M., Pitte, P., Popovnin, V. V., Portocarrero, C. A., Prinz, R., Sangewar, C. V.,
871 Severskiy, I., Sigurdsson, O., Soruco, A., Usabaliev, R., and Vincent, C.: Historically



872 unprecedented global glacier decline in the early 21st century, *Journal of Glaciology*, 61, 745–
873 762, <https://doi.org/10.3189/2015JoG15J017>, 2015.

874 Zemp, M., Huss, M., Thibert, E., Eckert, N., McNabb, R., Huber, J., Barandun, M., Machguth,
875 H., Nussbaumer, S. U., Gärtner-Roer, I., Thomson, L., Paul, F., Maussion, F., Kutuzov, S., and
876 Cogley, J. G.: Global glacier mass changes and their contributions to sea-level rise from 1961
877 to 2016, *Nature*, 568, 382–386, <https://doi.org/10.1038/s41586-019-1071-0>, 2019.